Experimental and theoretical investigations of some useful langasite cuts for high-temperature SAW applications

Jochen Bardong, Thierry Aubert, Natalya Naumenko, Gudrun Bruckner, Sabine Salzmann, Leohnard M. Reindl

Experimental and Theoretical Investigations of some Useful Langasite Cuts for High-Temperature SAW Applications

Jochen BARDONG[1], Thierry AUBERT[1], Natalya NAUMENKO[2], Gudrun BRUCKNER[1], Sabine SALZMANN[1], Leonhard M. REINDL[3]

[1] Carinthian Tech Research, Villach/St. Magdalen, Austria
[2] Moscow Steel and Alloys Institute, Acoustooptics Center, Russia
[3] Laboratory of Electrical Instrumentation, Department of Microsystems Engineering (IMTEK), Albert-Ludwigs-Universität, Freiburg, Germany

Abstract— **Passive high-temperature sensors are a most promising area of use for surface acoustic wave (SAW) devices. Langasite ($La_3Ga_5SiO_{14}$, LGS) has been identified as promising piezoelectric material to meet high-temperature SAW challenges. As it is necessary to know the material behavior for an accurate device design, the frequency-temperature behavior of Rayleigh SAW (R-SAW) and shear horizontal SAW (SH-SAW) LGS cuts is investigated on delay line and resonator test structures up to 700°C by RF characterization. In the range of the 434 MHz-ISM band, the (0°, 22°, 90°) SH-SAW cut shows similar thermal behavior as the (0°, 138.5°, 26.7°) R-SAW cut. Associated with the (0°, 22°, 31°) cut, in which SAW present mixed type of polarization, the (0°, 22°, 90°) SH-SAW orientation might allow differential measurements on one single substrate. In the temperature range of 400 to 500°C, delay line test devices using the SH-SAW cut show a considerable drop of signal. Theoretical analysis evidences that this newly described behavior might be a result of anisotropy effects in this cut, occurring in case of any slight misorientation of electrode alignment.**

Keywords-high temperature; SAW; SH-SAW; langasite; sensor

I. INTRODUCTION

As surface acoustic wave (SAW) devices are very sensitive to external conditions like temperature or pressure, while being passive, they offer the possibility to realize wireless sensors that could operate in high-temperature conditions for long time periods [1]. During the last decade, many efforts have been made to identify and characterize piezoelectric materials that could be used in such conditions. Indeed,

conventional SAW substrates, such as quartz, lithium niobate or lithium tantalate, are all limited to temperatures below 500°C because of intrinsic physical or chemical transformations [2]. Up to now, the most reliable results concerning device stability and reproducibility have been obtained with langasite ($La_3Ga_5SiO_{14}$, abbreviate as LGS). Thus, a SAW signal was recently recorded up to 1140°C by Aubert *et al.* [3], while Pereira da Cunha *et al.* have successfully operated LGS-based SAW devices for several months at 800°C [4]. So, LGS is currently the best-suited piezoelectric material for high-temperature SAW applications taking into account availability of crystals and different orientations, too. Nowadays, a major task is to find the crystal cuts and orientations appropriate for specific purposes. Up to now, the prediction of cuts fitting dedicated needs is numerically inaccurate as the available LGS material tensor sets are incorrect above 250°C [5-6]. In order to improve existing data sets, the presented study examines experimentally the frequency-temperature laws of three different LGS cuts in the temperature regime between the ambient and 700°C. For this investigation, the following LGS cuts have been chosen, as they provide sufficiently high electromechanical coupling coefficient K^2 and zero power flow angle: the (0°, 138.5°, 26.7°) Rayleigh SAW (R-SAW) cut, which is the most extensively examined LGS cut up to now, the shear horizontal SAW (SH-SAW) cut with Euler angles (0°, 22°, 90°), and the (0°, 22°, 31°) cut which presents mixed type of polarization [6-9]. All crystals were processed with delay line devices as well as with resonator structures using the same device mask. The pitch is 2.4 µm and 3.3 µm for the delay line and the resonator test structures respectively. A platinum based multilayer with a total thickness h of 120 nm was developed and applied to the crystals to enable the electrodes to withstand elevated temperatures of estimated 900°C.

In the second section, the SAW devices and experimental methods used to examine these substrates are described. During the third section, the experimental results are presented and discussed, whereas in the fourth section, theoretical investigations aiming at the explanation of several experimental observations on the (0°, 22°, 90°) SH-SAW cut are given. The conclusions are presented in the fifth section.

II. EXPERIMENTAL METHODS

The investigations were done mainly by S-parameter measurements on delay lines. A description of the setup dedicated to *in situ* RF high-temperature measurements can be found in [10]. The delay lines examined during this study provide four operating frequencies ranging from 140 MHz to 530 MHz by combining two interdigital transducers (IDTs), called here IDT A and B, with different frequency splitting. This allows the use of identical pitches for both IDTs, which reduces the mask complexity. IDT A is designed to work at frequencies of 1/4, 3/4, 5/4 and 7/4, whereas IDT B shows its harmonic frequencies at 3/7, 5/7, 9/7 and 11/7 of the center frequency f_0 (Fig. 1). This center frequency f_0 corresponds to an imaginative standard IDT with used finger pitch of 2.4 µm and can be located at about 600 MHz, differing slightly from cut to cut according to different propagation velocities of the excited waves [11-12].

Because of the high mass loading of R- and SH-SAW waves under a platinum based metallization, a large part of the energy of the highest harmonic frequencies, i.e. those above f_0, is lost. This resulted in four reliable signals per test device, where each IDT contributed with two harmonics (Fig. 2): 1/4, 4/7, 3/4 and 6/7 of f_0, corresponding respectively to relative thicknesses of 0.625%, 1.43%, 1,875% and 2.14%.

The frequency-temperature behavior of the examined LGS cuts was determined by heating the samples continually from room temperature to 900°C (temperature ramp: 100°C/h) in fine vacuum conditions (pressure = $2*10^{-4}$ mbar). Due to this ramp slope, a measurement could be done with 1 Kelvin difference between start and end of a frequency sweep and it was steep enough to shift the device failure to temperatures above 850°C. With a ramp less steep, dewetting processes starting at temperatures above 700°C on Pt based layers, have more time to impact the metallization which leads to stronger signal disruption and device failure at temperatures below 850°C.

Concerning the (0°, 22°, 90°) SH-SAW cut, the measurement results were reproducible, but inconclusive. So, a counter-check using a one-port synchronous resonator structure, with a pitch of 3.3 µm, was added to clarify the behavior of this cut. These resonators were measured in the same way as the delay line test structures mentioned above.

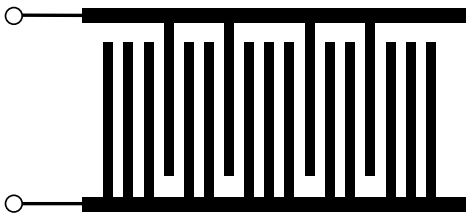

Fig. 1. Electrode pattern of the IDT with N/7th harmonic splitting

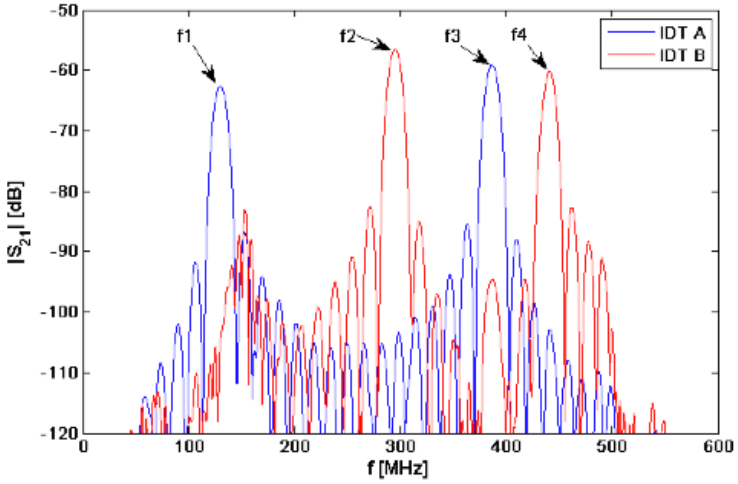

Fig. 2. Frequency responses of IDTs A and B with platinum electrodes

III. MEASUREMENT RESULTS AND DISCUSSION

The two cuts (0°, 138.5°, 26.7°) and (0°, 22°, 31°) give reliable results until temperatures up to 700°C (Fig. 3 and 4). At temperatures above this mark, the deviation from the fitting parabola curve is getting significant and is accompanied by an irreversible signal amplitude degradation, which increases with operating frequency. That can be explained by two main effects: one is the starting agglomeration and dewetting of the Pt electrodes from this temperature on [13]. The other effect is an increasing surface roughness of LGS substrates at high temperatures under low-pressure environments [3,14]. Waves with higher frequencies and therefore shorter wavelengths λ have a smaller surface penetration depth which makes them more sensitive to any change in surface and electrode roughness. The cavities described in [14] that can be observed all over the crystal surface appear during the heating process. They grow in the scale of several micrometers and work as diffraction centers for a passing SAW. The diffracting effect

rises as the wavelength shrinks and its penetration depth reaches the cavities extent. Fig. 5(a)-(d) give an impression of the degradation effects.

The relative thickness h/λ of the electrodes also demonstrated an increasing influence on the frequency-temperature law with rising temperature. Related to the strengthening with temperature of the IDTs mass loading, this effect is understood and predictable by simulation methods, as it can impact the performance of SAW filters used in telecommunication devices considerably [15]. In the case of SAW devices operating in high-temperature environments, it was observed that this phenomenon influences strongly the device behavior for some cuts. For instance, in case of the (0°, 22°, 31°) cut, the observed thermally induced frequency shift between room temperature and 600°C is smaller by 2500 ppm at 440 MHz (h/λ = 2.14%) compared to the observed shift at 130 MHz (h/λ = 0.62%) (Fig. 4).

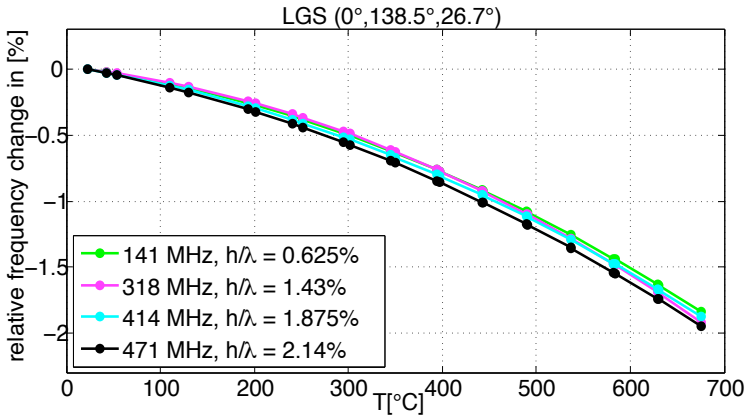

Fig. 3. Experimental frequency-temperature laws of (0°, 138.5°, 26.7°) LGS cut

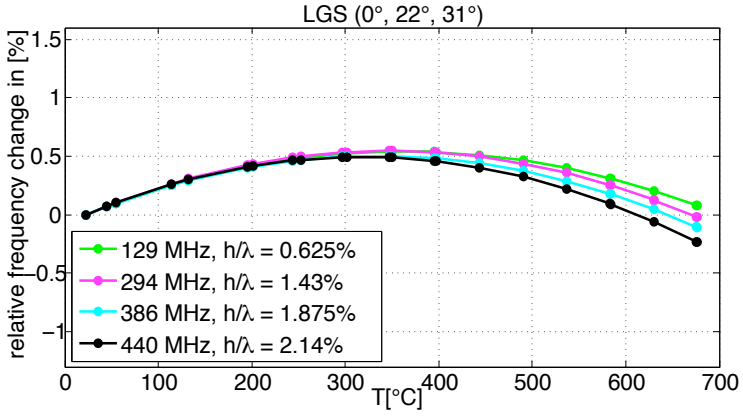

Fig. 4. Experimental frequency-temperature laws of (0°, 22°, 31°) LGS cut

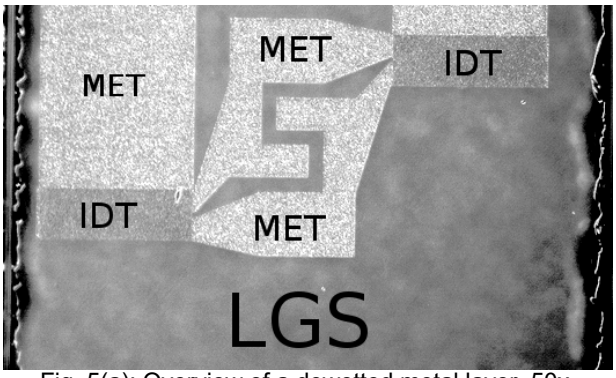

Fig. 5(a): Overview of a dewetted metal layer, 50x enhancement in optical microscope. The IDT structures are still recognizable as are the formerly closed metal layers of this delay line with metalized propagation path (noted as MET).

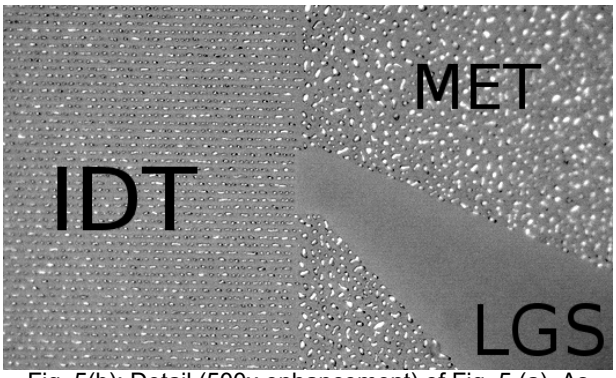

Fig. 5(b): Detail (500x enhancement) of Fig. 5 (a). As can be recognized, the IDT structure and the formerly closed metal layer have been separated into isolated droplets during the annealing process.

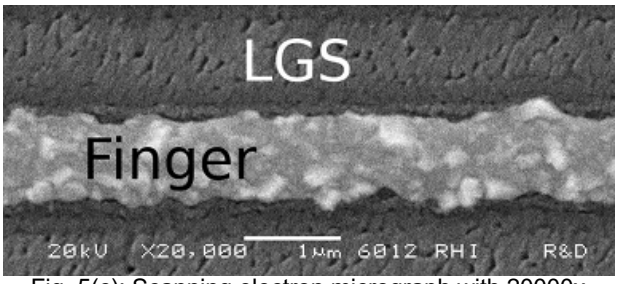

Fig. 5(c): Scanning electron micrograph with 20000x enhancement of an IDT finger and LGS surface in between. The surface shows several micro fissures, the finger beginning dewetting as can be recognized in agglomeration and deformation.

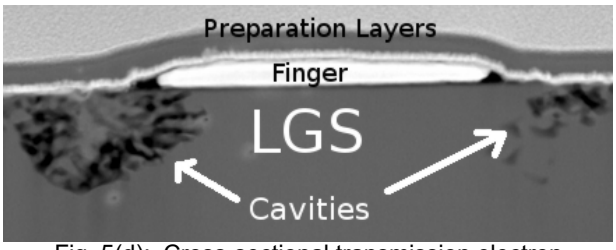

Fig. 5(d): Cross-sectional transmission electron micrograph with 40000x enhancement of an IDT finger and its adjacent LGS surrounding. The fissures from Fig. 5 (c) seem to be the top view of deeper cavities. The finger has a width of 1.2 µm so the left cavity is about 500 nm in depth. On top of the surface is a preparation layer necessary to perform the cross-sectional preparation.

Thus, to compare the temperature behavior of the different cuts, it is mandatory to use devices with operating frequencies as close as possible to each other and devices of equal design. Therefore, the formerly presented delay lines can be considered as a good possibility to do so.

Unfortunately the analysis of the signals deduced from delay lines on the (0°, 22°, 90°) SH-SAW cut remained inconclusive. In the 400-500°C regime, a clearly reproducible signal drop occurs, disabling the evaluation algorithm to track the signal amplitude, which causes a jump in the trend lines of Fig. 6. Outside this temperature area, the signal amplitude was analyzable. However, the material degradation effects like dewetting and crystal decomposition on the SH-SAW cut were comparable to those observed on the two other cuts.

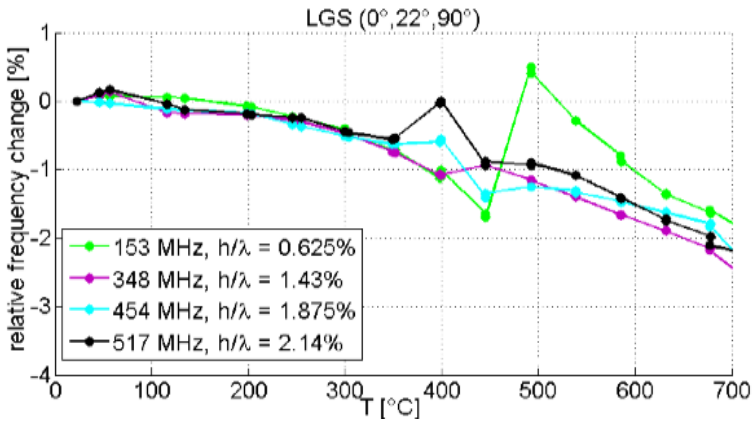

Fig. 6. Experimental frequency-temperature laws of SH-SAW (0°, 22°, 90°) LGS cut

Thus, signals were thoroughly analyzed via spectrograms. This signal representation shows the signal energy distribution in the time-frequency plane. Thereby, the transfer function and impulse response are projections of the spectrogram pattern versus the abscissa or ordinate, respectively. That kind of projection leads to a loss of detail and buries signal amplitudes that have the same frequency but different propagation times, for example. In Fig. 7, a spectrogram of the (0°, 138.5°, 26.7°) R-SAW cut at room temperature is presented. The coloring code is such that areas of rising energy are colored from yellow to red whereas areas of low and decreasing energy close to the noise floor are colored from green to blue. The concentrated red areas correspond to frequency-time events with highest signal energy, i.e. to the main lobes of a dedicated harmonic where constructive wave excitation and propagation is achieved. There are two main lobes per frequency (abscissa) at different times (ordinate). It indicates both delay lines with different lengths per chip that were electrically added for compact signal measurement and analysis. Periodically repeated orange-red dots between two harmonic frequencies at identical times correspond to sidelobes of the sinc^2 function, the Fourier transform of rectangular designed IDTs. In time domain, no sidelobe is expected, as the signal consists here of two convolved rectangles which results in a triangularly formed maximum. Parasitic wave modes that are excited and transmitted across the delay line propagation path and/or partly through the crystal bulk material are marked by circles. They show up in between and close by the designed main lobes, distorting the transfer function as well as the impulse

response. When inspecting the transfer function only, which is the projection of the spectrogram energy distribution to the abscissa, most of these encircled spurious signals in Fig. 7 would be invisible. A spectrogram of a delay line on the (0°, 22°, 90°) SH-SAW cut at room temperature is shown in Fig. 8. Compared with the spectrogram of the (0°, 138.5°, 26.7°) R-SAW cut, many highly energized spurious modes can be detected. This indicates that with delay lines and IDTs using spatial sampling, numerous unwanted modes are excited in addition to the SH-SAW wave modes. Some of the observed parasitic modes can be identified as bulk acoustic wave modes (BAW), like those in the big circle in the upper left of Fig. 8. This group of BAW modes shows a characteristic shift in time and frequency from one energy maximum to the next leading to a stairway-like pattern**.** The BAW are emitted and generated inside the IDT, become reflected between top and bottom of the crystal and transverse the propagation path from the input IDT in a zigzagging manner between crystal surface and bottom towards the receiving IDT**.** The higher the number of zig-zag reflections, the longer the transmission time and the shorter the wavelength, as the latter is dependent on the angle θ between surface and propagation direction of the BAW (Fig. 9) [16]. Other marked modes visible on Fig. 8 are more complex to interpret, which is beyond the scope of this text.

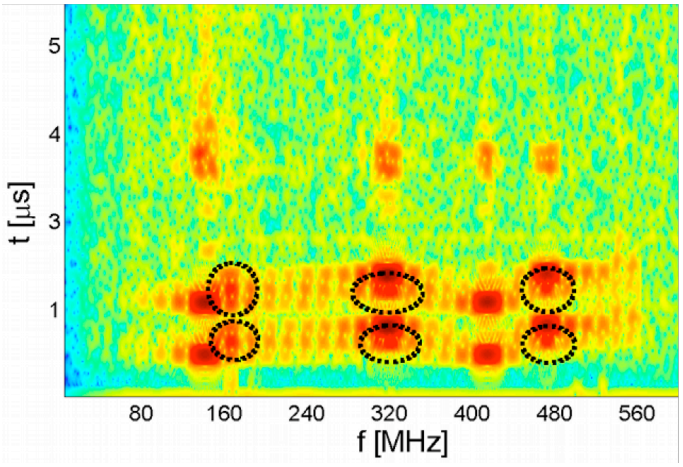

Fig. 7. Spectrogram of (0°, 138.5°, 26.7°) LGS cut at 28°C. Parasitic signals are marked by circles.

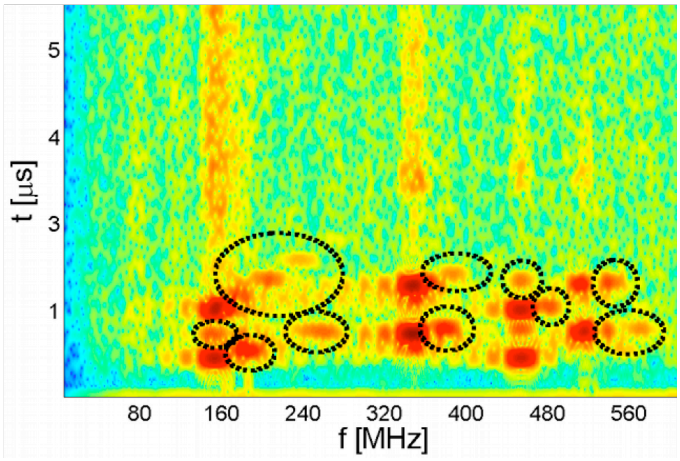

Fig. 8. Spectrogram of SH-SAW (0°, 22°, 90°) LGS cut at 28°C. Parasitic signals are marked by circles.

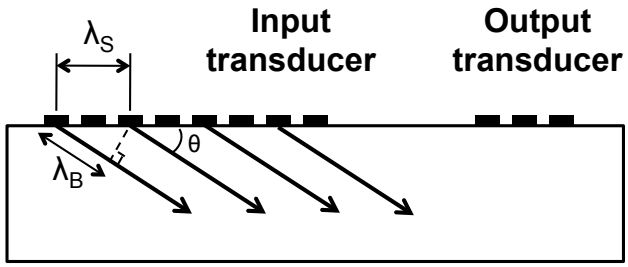

Fig. 9. Bulk wave generation by interdigital transducers. The wavelength of the BAW, λ_B, is shorter than λ_S, which is the one of the dedicated SAW. Both are related by the relation $\lambda_B = \lambda_S.\cos\theta$

Between 400 and 500°C, spectrograms corresponding to the (0°, 22°, 90°) SH-SAW cut confirm a considerable signal drop that occurs at all observed harmonic frequencies, with some differences in intensity (Fig. 10). The effect has a stronger impact on the designed IDT harmonics than for the spurious modes. The amplitude energy of several IDT harmonics decreases with rising temperature and drops to a comparable level like that of the neighboring parasitic modes at about 400°C. During the thermal translation from 400°C to 500°C, these parasitic modes grow in amplitude whereas that of some designed IDT harmonics falls below noise level. Above 500°C, the main harmonics recover to a signal level above that one of the spurious mode (Fig. 11). Compared to that effect, the spectrograms from devices on (0°, 138.5°, 26.7°) (Fig. 12) and (0°, 22°, 31°) cuts do not show any kind of mode conversion in this temperature regime.

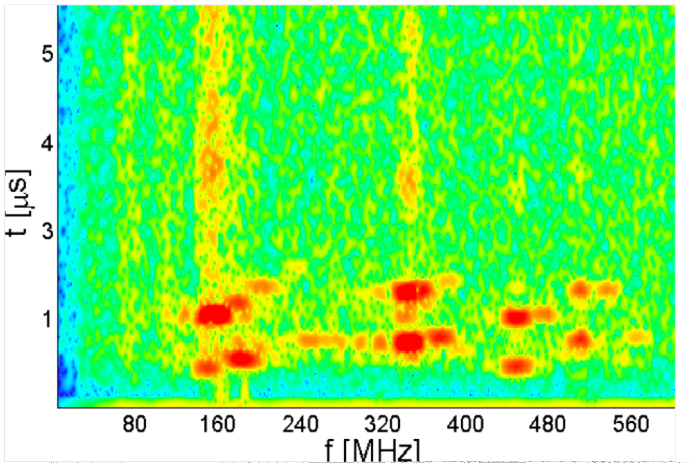

Fig. 10. Spectrogram of SH-SAW (0°, 22°, 90°) LGS cut at 440°C.

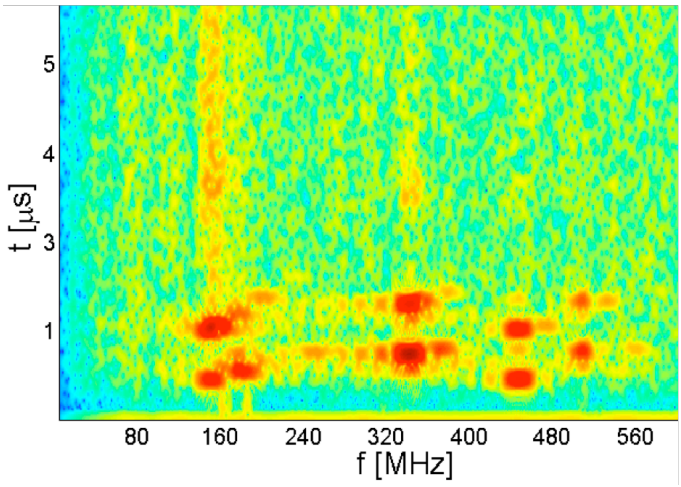

Fig. 11. Spectrogram of SH-SAW (0°, 22°, 90°) LGS cut at 580°C.

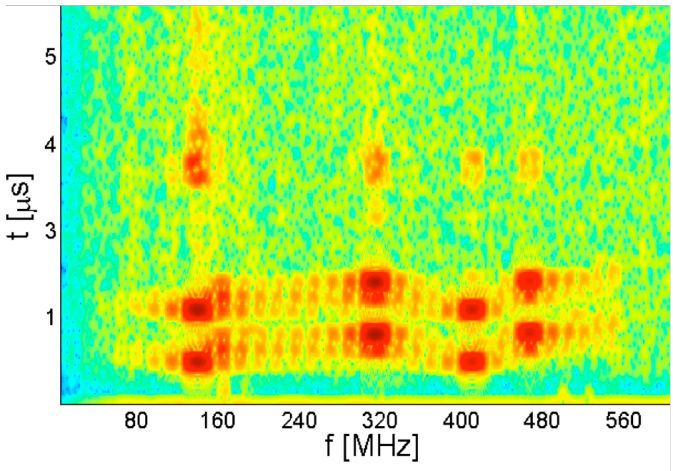

Fig. 12. Spectrogram of R-SAW (0°, 138.5°, 26.7°) LGS cut at 440°C.

At temperatures above 580°C, the signals of the (0°, 138.5°, 26.7°) and the (0°, 22°, 31°) cuts decrease gradually, according to expected propagation losses, and signal analysis remains possible over the whole temperature sweep (Fig. 13). Despite these new information provided by the use of the spectrograms, the results about the (0°, 22°, 90°) SH-SAW cut were still not easily understandable.

The inconclusive results from the delay line signal analysis on the (0°, 22°, 90°) SH-SAW cut were then completed by additional measurements using synchronous resonator test structures. Fig. 14 shows the evolution of the corresponding Bode plot (S_{11} magnitude and phase) over the investigated temperature range. Due to the lack of calibration possibilities and total cable lengths of 3 meters leading to strong insertion losses and signal phase distortion effects, a considerable part of the information was lost. However, it was observed that, in contrast to delay line measurements, the resonator signal is stable over the temperature regime between 400 and 500°C. Above this temperature, the signal magnitude decreases gradually, which prevents an accurate determination of the evolution of the synchronous frequency (Fig. 14(a)). Thus, the frequency-temperature behavior of devices was extracted via phase tracking measurements (Fig. 14(b)). Reproducible results were then obtained, removing the uncertainty about the thermal behavior of the (0°, 22°, 90°) SH-SAW cut between 400 and 500°C (Fig. 15). The results are consistent with data from Sakharov *et al.* [17].

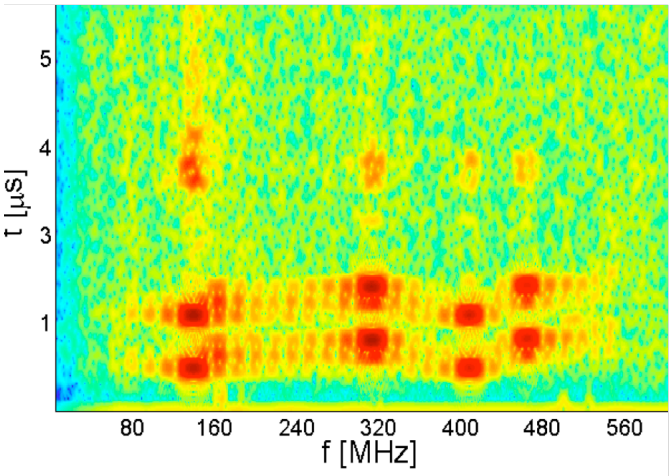

Fig. 13. Spectrogram of (0°, 138.5°, 26.7°) LGS cut at 580°C.

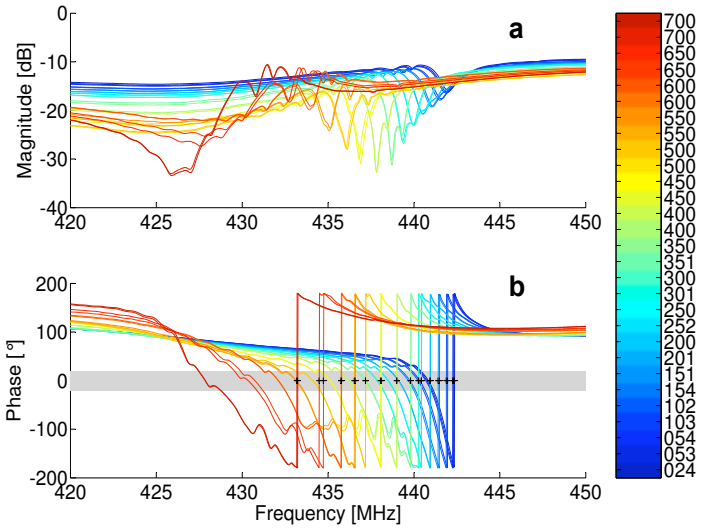

Fig. 14. Evolution with temperature of S_{11} magnitude (a) and phase (b) of a typical SAW resonator built on SH-SAW (0°, 22°, 90°) LGS cut. Temperature is given by the color scale on the right. The phase plot is utilized to follow the frequency change with temperature via 0° tracking (see grey strip).

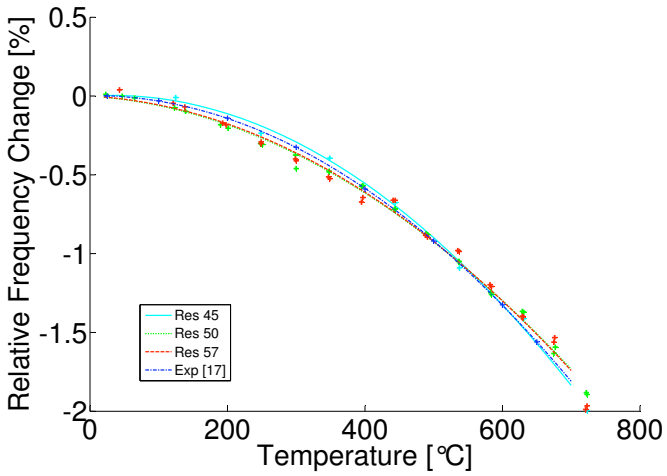

Fig. 15. Comparison between results obtained on 3 typical resonators built on the SH-SAW (0°, 22°, 90°) LGS cut, and those taken from [17].

With the data derived from the additional resonator measurements on the (0°, 22°, 90°) SH-SAW cut, the frequency-temperature behaviors of all examined cuts at frequencies close by the 434MHz ISM-band were compared (Fig. 16). Therefore some prospective applications may be suggested. Thus, the (0°, 22°, 90°) SH-SAW cut and the (0°, 138.5°, 26.7°) cut are characterized by similar temperature

coefficient of frequency (TCF) value trends, which are close to zero at room temperature. They can subsequently be considered both for applications requiring thermal compensation (e.g. non-temperature sensing) at ambient temperature assuming an appropriate choice of metal and thicknesses for the electrodes so that the TCF reaches effectively 0 ppm/°C [9]. In addition, providing a pure transversal wave mode, the (0°, 22°, 90°) SH-SAW cut appears to be ideal for liquid sensing [8]. Considering temperature sensing applications, the (0°, 22°, Ψ) cut seems to be a top candidate from ambient temperatures to 500°C, as in this temperature range, the orientations Ψ = 31° and Ψ = 90° have different temperature behaviors and could therefore be combined on one die to create a pair of sensors [6]. This allows differential measurement methods, required in resonator configurations as the RF link itself may notably affect the resonance frequency, with a minimized-size device [18].

IV. THEORETICAL INVESTIGATION OF THE (0°, 22°, 90°) SH-SAW LGS CUT

The experimentally observed unexpected features in the behavior of SH-SAW in the LGS cut (0°, 22°, 90°), described in the previous section, cannot be predicted with known models of SAW propagation in a substrate with IDTs or periodic gratings. Some of the spurious responses, which degrade the performance of experimental delay lines, can be referred to shear horizontal (SH) polarized BAW, which propagates with a velocity slightly higher than that of SH-SAW.

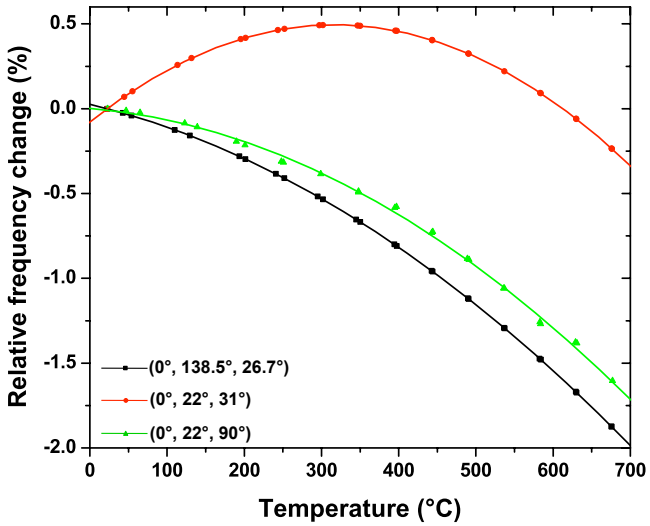

Fig. 16. Experimental frequency-temperature laws of the 3 investigated LGS cuts close to the 434 MHz ISM-band.

However, a more complete understanding of the observed phenomena is possible if the effect of anisotropy on the wave propagation in this cut is taken into account [19]. This cut belongs to the symmetric orientations described by the Euler angles (0°, θ, 90°), in which two degenerate SAW solutions can exist. One is the piezoelectrically coupled SH-SAW (also known as Bleustein-Gulyaev wave or surface transverse wave (STW) when it propagates in a periodic grating), with SH polarization along X-axis of LGS. The second one is the uncoupled Rayleigh wave polarized in the sagittal plane, i.e. YZ plane of LGS. The velocities of those two modes are generally different.

Any deviation from a symmetric cut, e.g. misorientation caused by technological errors, eliminates degeneracy of SAW solutions and results in a transformation of each mode into the generalized SAW or leaky wave with mixed type of polarization. The electromechanical coupling of the Rayleigh-type mode slowly grows with such a deviation. When misorientation does not exceed 0.5° and the velocities of both modes are substantially different, the influence of the Rayleigh-type SAW on the device performance is negligible. A specific feature of the LGS cut (0°, 22°, 90°) is that both modes propagate here with nearly the same velocity. Therefore, even a small deviation from symmetric orientation is followed by a strong interaction between the modes, which affects the device performance.

Fig. 17 shows the velocities of SH-type and Rayleigh-type SAWs arising nearly from the same velocity point when the propagation direction deviates by the angle ψ from the YZ plane towards the X-axis of LGS. These and further calculations were made with LGS constants reported in [20]. In Fig.17, metalized surface is considered, which is equivalent to short-circuit electrical boundary conditions on the surface. If ψ=0, the velocities of both SAWs are slightly smaller than V_{BAW}, i.e. the velocity of the bulk acoustic wave propagating along the surface with a wave vector generally tilted into the bulk [19]. With increasing ψ, SH-SAW holds its quasi-bulk nature. Rayleigh-type SAW transforms into leaky SAW when ψ>0.5°, and its attenuation coefficient grows fast with ψ.

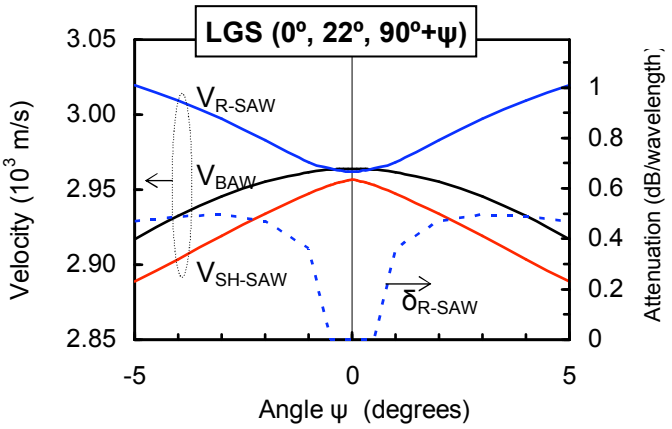

Fig. 17. Velocities of SH-type (red line) and Rayleigh-type surface waves (blue line) and attenuation of Rayleigh-type leaky SAW (dashed line) in LGS orientations with Euler angles (0º, 22º, 90º+ψ), as functions of the angle ψ. The black line refers to SH-BAW velocity.

With the deposition of a metal film or a periodic metal grating of finite thickness, the velocities of both modes decrease, but the difference between them stays small as long as $\psi<0.5°$. For example, Fig. 18 shows the variation of effective velocities of both SAW modes in orientation (0°, 22°, 90.1°) with periodic metal grating, as functions of the normalized electrode thickness $h'=h_{el}/2p$. Platinum electrodes (h_{Pt}=100 nm) with titanium sublayer (h_{Ti}=10 nm) and a variable pitch of the electrode structures, p=3…10 μm, have been considered. These parameters are consistent with the experimental devices. The effective velocities were calculated in short-circuit (SC) and open-circuit (OC) gratings as $V_R=2pf_R$ and $V_A=2pf_A$, respectively, where f_R and f_A are resonant and anti-resonant frequencies extracted from numerically derived admittance functions $Y(f)$. The velocities V_R and V_A refer to SH-type SAW propagating in a periodic grating. Rayleigh-type mode is also trapped by the grating and builds its own reflection stopband. The velocities $V_1=2pf_1$ and $V_2=2pf_2$ refer to the edges of this stopband, f_1 and f_2, which are nearly the same for SC and OC electrical conditions, because of the low piezoelectric coupling of the Rayleigh-type SAW. As the influence of electrode thickness is smaller on Rayleigh-type than on SH-SAW, $f_1(h')$ and $f_2(h')$ dependences cross $f_R(h')$ and $f_A(h')$ when the normalized electrode thickness increases. Each intersection means that the two SAW modes propagate with equal velocities and the interaction between them grows dramatically.

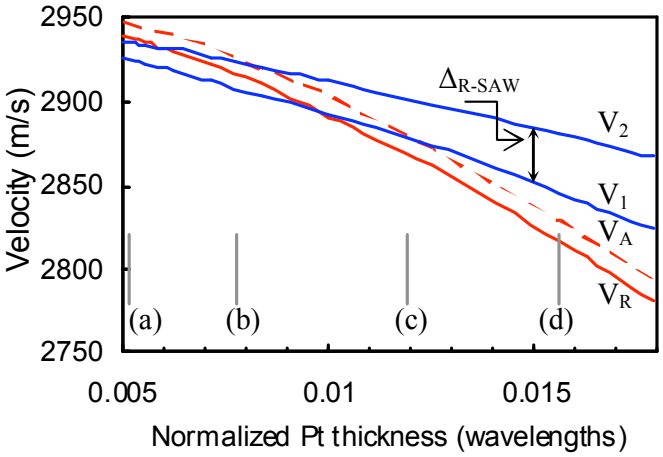

Fig. 18. Effective SH-SAW velocities at resonant (V_R) and anti-resonant (V_A) frequencies, and velocities $V_{1,2}$ indicating the edges of Rayleigh-type SAW stopband, $\Delta_{R\text{-}SAW}$, in Ti/Pt grating on LGS cut (0º, 22º, 90.1º), as functions of the normalized Pt thickness. The labels (a)-(d) refer to the periods of the grating analyzed in Fig. 19.

This is illustrated by the normalized admittance functions $Y(f)/Y(0)$ (Fig. 19) obtained at four values of electrode thickness, labeled in Fig. 18 as (a)-(d). When the pitch decreases from 9.6 μm to 3.2 μm, the stopband of the spurious mode moves from the frequencies $f_{1,2}<(f_R, f_A)$ [Fig. 19(a)] to the frequencies $f_{1,2}>(f_R, f_A)$ [Fig. 19(d)]. If p=6.4 μm [Fig. 19(b)], then f_2 occurs between f_R and f_A. If p=4.2 μm [Fig. 19(c)], then f_1 is confined in the interval (f_R, f_A). Maximum effect of the spurious mode on the resonant frequency is expected for $p\approx$5 μm and $p\approx$8.5 μm. The anti-resonant frequency will be perturbed most strongly if $p\approx$3.9 μm and $p\approx$5.8 μm.

When the working temperature rises, the velocities V_R, V_A, V_1 and V_2 all decrease. SH-SAW is characterized by nearly zero TCF in the cut (0°, 22°, 90°) whereas the spurious mode shows stronger dependence on temperature. As a result, the intersections between the velocities of the two SAW modes occur at temperatures which depend on the electrode pitch. For instance, if p=3.2 μm (which corresponds to $f \approx$ 440 MHz, close to the ISM-band), the admittance looks nearly perfect when T=25°C [Fig. 19(d)]. The interaction between the modes occurs at higher temperatures, when $f_R(T)$ and $f_A(T)$ are crossed by $f_1(T)$, as shown in Fig. 20, where misorientation ψ=0.1° is assumed.

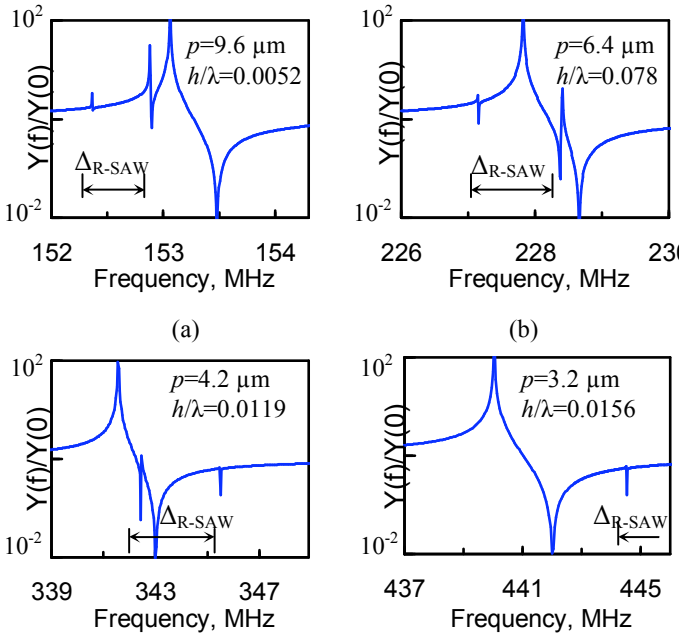

Fig. 19. Admittance of infinite grating with Ti/Pt electrodes on LGS cut (0º, 22º,90.1º), h_{Pt}=100 nm, h_{Ti}=10 nm, and different pitches of electrode structure: (a)-(d) refer to the normalized thicknesses labeled in Fig. 18. Two parasitic resonances occur at the edges of the stopbands built by Rayleigh-type SAW, $\Delta_{R\text{-}SAW}$.

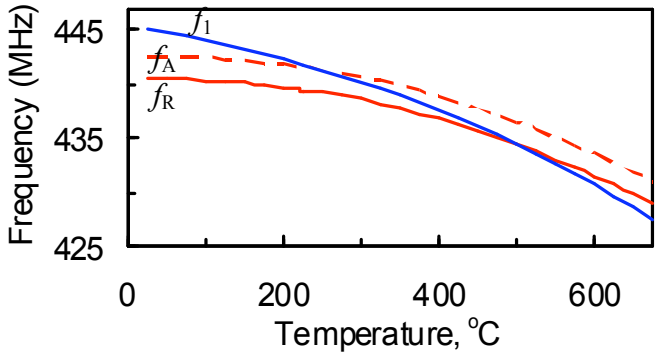

Fig. 20. Calculated resonant (f_R) and anti-resonant (f_A) frequencies of SH-SAW and resonant frequency of Rayleigh-type SAW at its lower stopband edge (f_1) in Ti/Pt grating with pitch p=3.2 μm, on LGS cut (0º, 22º, 90.1º), as functions of temperature.

Fig. 21 illustrates how the lower edge of the Rayleigh-type SAW stopband f_1 moves with respect to f_R and f_A when temperature increases from 25° to 650°C. When T=250°C, then $f_1 \approx f_A$ and anti-resonance looks split because of the strong interaction between the modes. At higher temperatures, f_1 is confined between f_R and f_A. A maximum effect of the parasitic mode on the resonant frequency is expected at

T≈500°C. Thus, it can be assumed that the signal drop observed with delay lines experimentally between 400 and 500°C is related to this interaction between the SH-SAW and the spurious SAW mode. However, the fact that the phenomenon is largely more intense with these devices than with the investigated resonator structures remains currently unexplained.

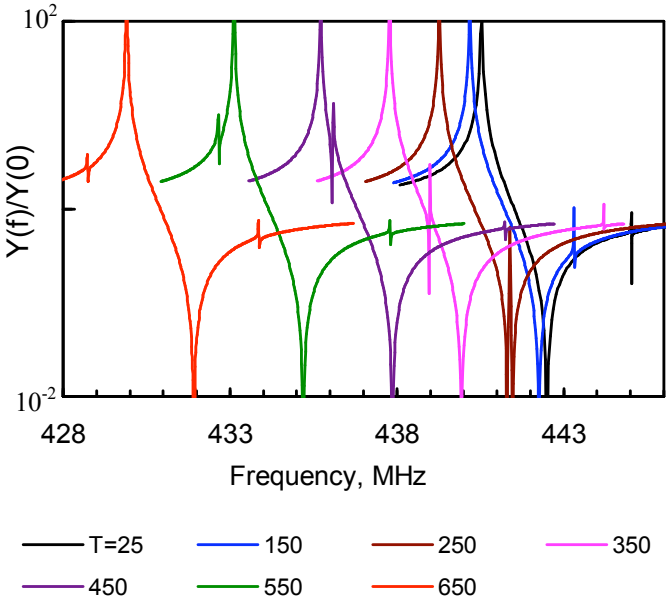

Fig. 21. Variation of the admittance of resonators with Ti/Pt electrodes and a pitch *p*=3.2 µm on LGS cut (0º, 22º, 90.1º) with temperature increasing from 25° to 650°C.

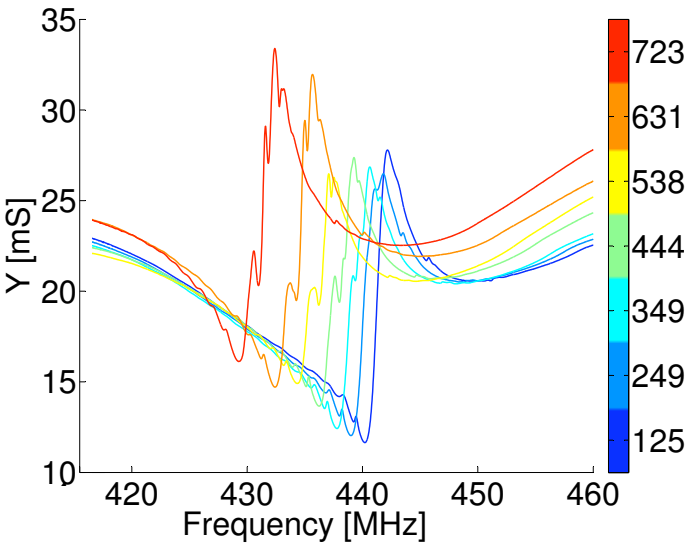

Fig. 22. Evolution with temperature of the measured admittance of a typical investigated resonator built on SH-SAW (0°, 22°, 90°) LGS cut. Temperature is given by the color scale on the right.

It should be mentioned that though theoretical analysis of the spurious mode was performed at fixed deviation of propagation direction from symmetric orientation, ψ=0.1°, a further increase of angle ψ up to 0.5° does not give noticeable shift of the found intervals of pitches and temperatures, in which a maximum degradation of the device performance is expected. However, the piezoelectric coupling of the spurious mode increases with ψ.

The presence of a parasitic SAW, traveling with temperature, is experimentally observed on the admittance curves obtained from measurements performed on resonators (Fig. 22). At room temperature, the resonant and anti-resonant frequencies are located in the vicinity of 440 MHz and 442 MHz, respectively, whereas a weak spurious mode can be seen close to 445 MHz. This is in good agreement with the calculations (Fig. 20), as well as the fact that the parasitic SAW is more sensitive to temperature changes than the main mode. Consequently, the Rayleigh mode is located between resonance and anti-resonance from about 250°C on, which is also in good agreement with the simulation. Both peaks superpose when temperature is near 440°C, whereas it was expected around 500°C according to the calculations. This discrepancy could be caused by the lack of an accurate set of physical LGS constants for temperatures above 250°C and the ignored temperature dependence of Pt constants. The multiple spurious modes visible at frequencies above the parasitic SAW mode are caused by transversal modes inside the resonator structure, which propagate faster than the main SAW mode [21].

V. CONCLUSION

(0°, 22°, 90°) SH-SAW, (0°, 138.5°, 26.7°) R-SAW and (0°, 22°, 31°) langasite cuts have been experimentally investigated between room temperature and 900°C, via *in situ* electrical measurements. Both (0°, 138.5°, 26.7°) and (0°, 22°, 31) cuts show reliable results up to 700°C. Operating frequencies measured beyond this point are not relevant because of Pt electrode degradation and crystal decomposition. In the case of the SH-SAW cut, an intense drop in amplitude of the observed harmonic frequencies between 400 and 500°C, corresponding with a coincidental rise in amplitude of adjacent spurious modes occurs, which disables peak tracking of the delay line signal in that temperature regime.

The complete frequency-temperature law of this cut was then deduced via measurements conducted on resonator structures. It appears that the thermal behavior of this cut is very close to that of the (0°, 138.5°, 26.7°) orientation, with, in particular, a quasi-null TCF at room temperature. Such a property coupled to the shear-horizontal nature of the SAW propagating along the (0°, 22°, 90°) direction makes this cut an ideal candidate for liquid sensing. Moreover, this cut is also very promising to make resonator-based wireless temperature sensors working in high-temperature environments [22]. Indeed, if coupled to the (0°, 22°, 31°) cut, which has a turnover temperature close to 300°C, it could allow the fabrication of a pair of sensors and thus differential measurements on one single die, which is mandatory in a potential resonator configuration. But it has to be kept into account that any slight IDT misorientation on the (0°, 22°, 90°) cut leads to excitation of a spurious Rayleigh SAW mode with a velocity very close to that of the SH-SAW main mode. Consequently, coupling between these two modes occurs at dedicated temperatures depending on the relative electrode thickness, which leads to a serious degradation of the device performance. To avoid this, electrode thicknesses of $h_{Pt}/\lambda>2\%$ shall be considered for implementation [19] though such thicknesses of Pt layers must be carefully examined considering mass-loading and wave damping effects. Calculations show that such phenomena should happen at temperatures close to 500°C for devices working in the vicinity of the 434 MHz-ISM band, which might explain the observed signal drop on delay lines in that temperature region.

ACKNOWLEDGEMENTS

The authors would like to thank Alfred Binder, David Eisele and Elena Mayer for helpful discussions and suggestions during the work on this article. The measurements were partly carried out with SAW devices from the EU-SAWHOT project ([FP7/2007-2013]), grant agreement n°[NMP4-SL-2009-247821].

REFERENCES

[1] J. Hornsteiner, E. Born, G. Fischerauer and E. Riha, “Surface acoustic wave sensors for high-temperature applications,” in *Proc. IEEE Int. Freq. Control Symp.*, 1998, pp. 615-620.

[2] D. Damjanovic, "Materials for high temperature piezoelectric transducers," *Current Opinion in Solid State and Materials Science*, vol. 3, pp. 469-473, 1998.

[3] T. Aubert, J. Bardong, O. Elmazria, G. Bruckner and B. Assouar, “Iridium interdigital transducers for high-temperature surface acoustic wave applications,” *IEEE Trans. Ultrason. Ferroelectr. Freq. Control*, vol. 59, no. 2, pp. 194-197, Feb. 2012.

[4] M. Peireira da Cunha, R. J. Lad, T. Moonlight, G. Bernhardt and D. J. Frankel, “High temperature stability of langasite surface acoustic wave devices,” in *Proc. IEEE Ultrason. Symp.*, 2008, pp. 205-208.

[5] T. Aubert, F. Sarry, O. Elmazria *et al.*, “Extraction of COM parameters on Pt/LGS for high temperature SAW sensor,” in *Proc. IEEE Ultrason. Symp.*, 2008, pp. 820-823.

[6] S. Sakharov, S. Kondratiev, A. Zabelin, N. Naumenko, A. Azarov, S. Zhgoon and A. Shvetsov, “Theoretical and experimental investigation of langasite as material for wireless high temperature SAW sensors,” in *Proc. IEEE Ultrason. Symp.*, 2010, pp. 535-538.

[7] J. Koskela, S. Lehtonen, V. P. Plessky and M. M. Salomaa, " Surface transverse waves on langasite," *Appl. Phys. Lett.*, vol. 72, pp. 2665-2667, 1998.

[8] E. Berkenpas, S. Bitla, P. Millard and M. Pereira da Cunha, “Pure shear horizontal SAW biosensor on langasite,” *IEEE Trans. Ultrason. Ferroelectr. Freq. Control,* vol. 51, no. 11, pp. 1404-1411, Jul. 2004.

[9] N. F. Naumenko and L. Solie, “Optimal cuts of langasite, $La_3Ga_5SiO_{14}$ for SAW devices,” *IEEE Trans. Ultrason. Ferroelectr. Freq. Control*, vol. 48, no. 2, pp. 530-537, Mar. 2001.

[10] J. Bardong, G. Bruckner, G. Franz *et al.*, “Characterisation setup of SAW devices at high temperatures and ultra high frequencies,” in *Proc. IEEE Int. Freq. Control Symp.*, 2009, pp. 28-32.

[11] H. Engan, “Surface acoustic wave multielectrode transducers,” *IEEE Sonics Ultrason.*, vol. 22, no. 6, pp. 395-401, Nov. 1975.

[12] C.K. Campbell, P.J. Edmonson and J.S. Papa, “Multi-band SAW filter design using the Remez exchange algorithm,” in *Proc. IEEE Ultrason. Symp.*, 1983, pp. 1-4.

[13] T. Aubert, O. Elmazria, B. Assouar, L. Bouvot, M. Hehn, S. Weber, M. Oudich and D. Geneve, “Behavior of platinum/tantalum as interdigital transducers for SAW devices in high-temperature environments,” *IEEE Trans. Ultrason. Ferroelectr. Freq. Control*, vol. 58, no. 3, pp. 603-610, Mar. 2010.

[14] J. Bardong, G. Bruckner, M. Kraft and R. Fachberger, “Influence of packaging atmospheres on the durability of high-temperature SAW sensors,” in *Proc. IEEE Ultrason. Symp.*, 2009, pp. 1680-1683.

[15] T. Pastureaud, R. Lardat, S. Chamaly, L. Pnavaire and S. Ballandras, “Prediction of the thermal sensitivity of surface acoustic waves excited under a periodic grating of electrodes,” *IEEE Trans. Ultrason. Ferroelectr. Freq. Control*, vol. 52, no. 8, pp. 1378-1383, Aug. 2005.

[16] D. P. Morgan, *Surface-wave devices for signal processing*, Amsterdam, AE: Elsevier, 1991.

[17] S. Sakharov, N. Naumenko, A. Zabelin and S. Zhgoon, “Characterization of langasite for application in high temperature SAW sensors,” in *Proc. IEEE Ultrason. Symp.*, 2011, *in press*.

[18] S. Ballandras, R. Lardat, L. Penavaire *et al.*, G. Heider, “Micro-machined, all quartz-package, passive wireless pressure and temperature sensor,” in *Proc. IEEE Ultrason. Symp.*, 2006, pp. 1441-1444.

[19] N. Naumenko, “Effect of anisotropy on characteristics and behavior of shear horizontal SAWs in resonators using langasite,” *IEEE Trans. Ultrason. Ferroelectr. Freq. Control*, vol. 59, no. 11, pp. 2515-2521, Nov. 2012.

[20] A. Bungo, C. Jian, K. Yamaguchi *et al.*, “Analysis of surface acoustic wave properties of the rotated *Y*-cut langasite substrate, ” *Jpn. J. Appl. Phys*., 1999, pp. 3239-3243.

[21] O. Schwelb, E. L. Adler and G. W. Farnell, “Effect of anisotropy on waveguide modes in SAW resonators,” in *Proc. IEEE Ultrason. Symp.*, 1977, pp. 867-872.

[22] E. Mayer, D. Eisele, L. M. Reindl *et al.*, "SAW parameters for langasite at high temperatures,” in *Proc. IEEE Ultrason. Symp.*, 2011, pp. 2069-2073.